Calculating the self-consistent vertical structure of a multicomponent stratospheric volcanic plume in a fine-resolution regional model

Georgiy Stenchikov, Alexander Ukhov, Sergey Osipov

King Abdullah University of Science and Technology (KAUST), Division of Physical Sciences and Engineering (PSE), Earth Sciences and Engineering Program (ErSE), Thuwal, Saudi Arabia

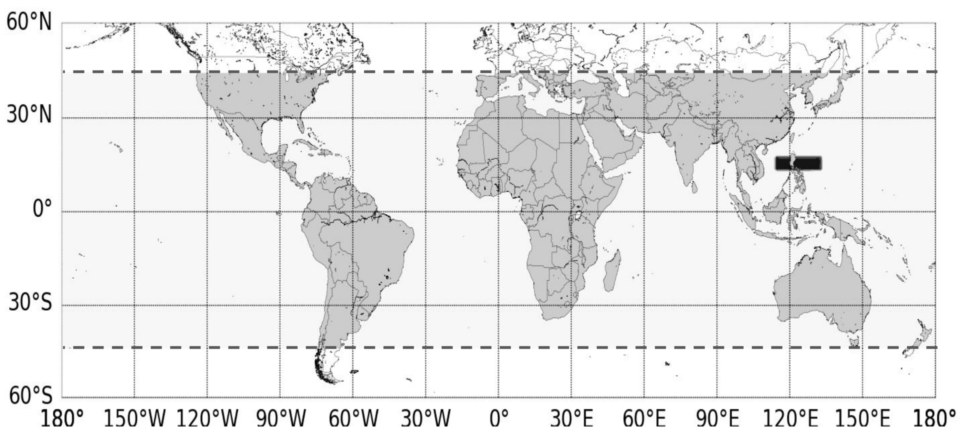

Fig. 1. Simulation domain (shaded area) and volcanic emissions. We assume that volcanic ash, SO_2, and water are injected into the "box" (1000x200x4 km^3) centered at the Mt. Pinatubo location at altitudes 17 and 24 km.

In this study we first time use regional model framework to study the impact of large explosive volcanic eruptions. We also first time account for the SO_2 radiative effect in SW and LW within a dynamic model. We use Mt. Pinatubo eruption parameters to consider the distinct effects of above-tropopause and middle-stratosphere volcanic emissions. We simulate here the initial two months of the volcanic plume evolution using a modified version of WRF-Chem v3.7.1 with GOCART aerosol module and RACM chemical mechanism in the equatorial belt domain with periodic boundary conditions in longitude (**Fig. 1**) and 100x100 km grid spacing using 401x111 grid points and 55 vertical levels with the top at 1 hPa (~42 km). We use the ERA-Interim Meteorological BC and the wind Spectral Nudging to reproduce QBO. The Ash Complex Refractive Index equals to 1.550+*i*0.001. The prescribed sulfate lognormal size distribution with r_{eff}=0.55μm used to account for gravitational settling. The GOCART Sulfur Cycle with interactive OH and nudged Ozone profile are employed to calculate the SO_2 to sulfate conversion. The 24 hours emissions comprise 17 Mt of SO_2, 75 Mt of Fine Ash, 100 Mt of Water (**Fig. 2 & 3**).

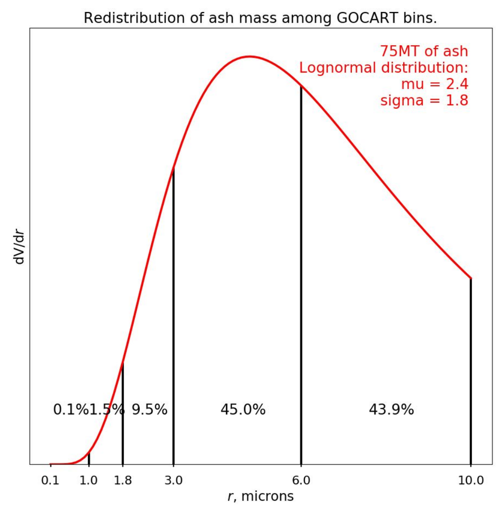

Fig. 2. Mass distribution of emitted fine ash into the GOCART size bins.

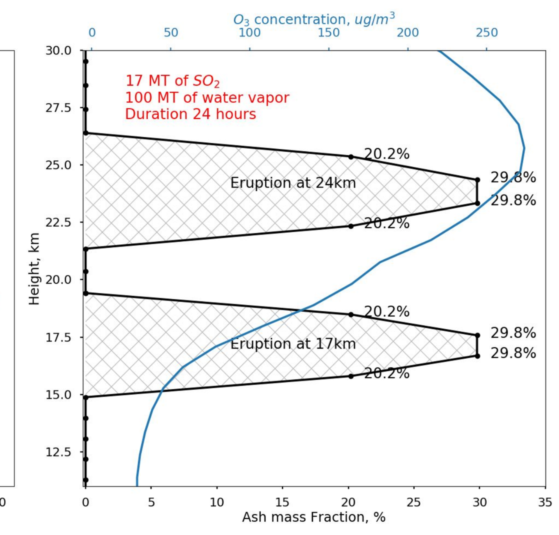

Fig. 3. Vertical mass distribution of emitted ash and SO_2. Blue line shows the prescribed profile of ozone (ug/m^3).

Eruption at 17 km with water emission

Eruption at 24 km without water emission

Eruption at 24 km with water emission

Fig. 4. Hovmoller diagrams of the lat-lon averaged within the equatorial belt concentrations (*ug/m^3*) of Ash, Sulfate, SO_2 and water. Solid contour lines correspond to the runs with the enabled sulfate, ash, SO_2 radiative feedbacks. Dashed contour lines correspond to the runs with the disabled radiative feedback.

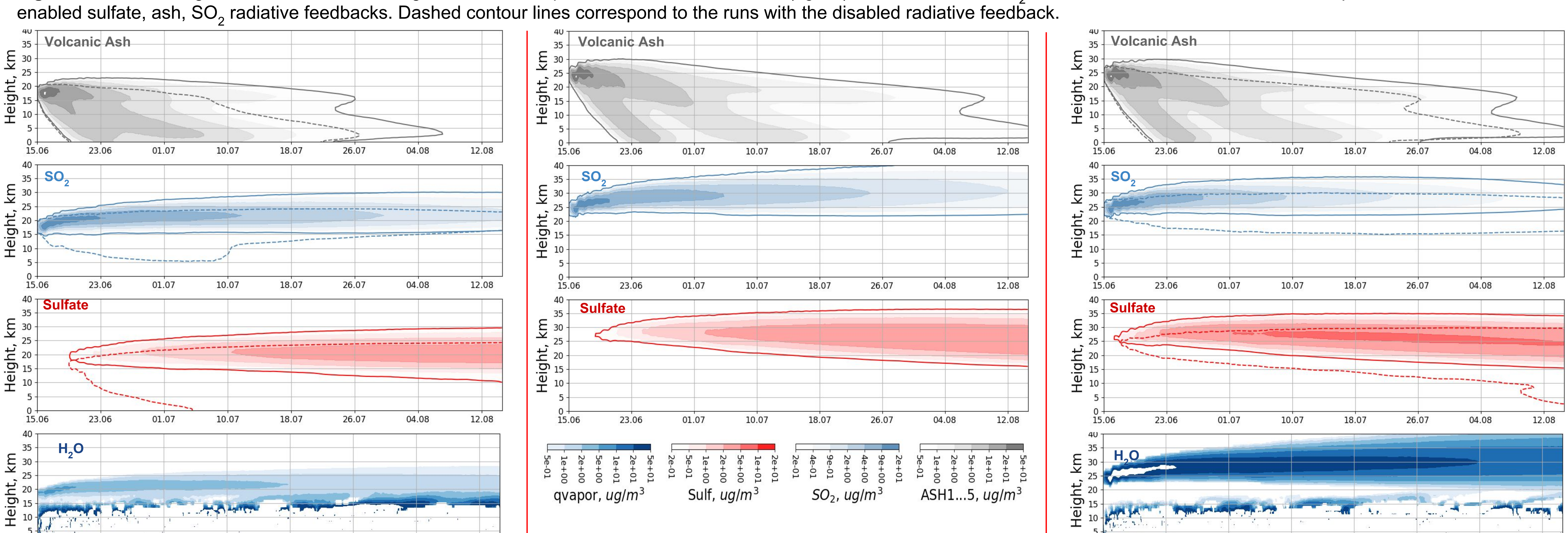

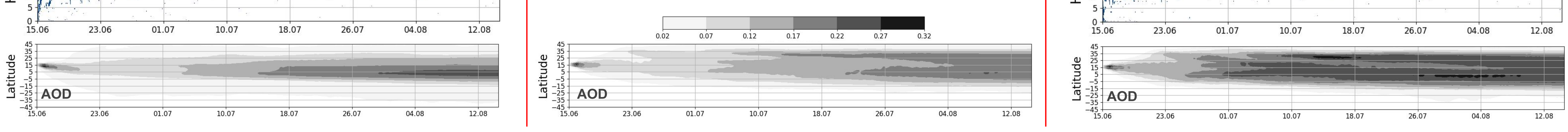

Fig. 5. Hovmoller diagram of zonally averaged total Aerosol Optical Depth (AOD) at 0.55 micron as a function of time and latitude.

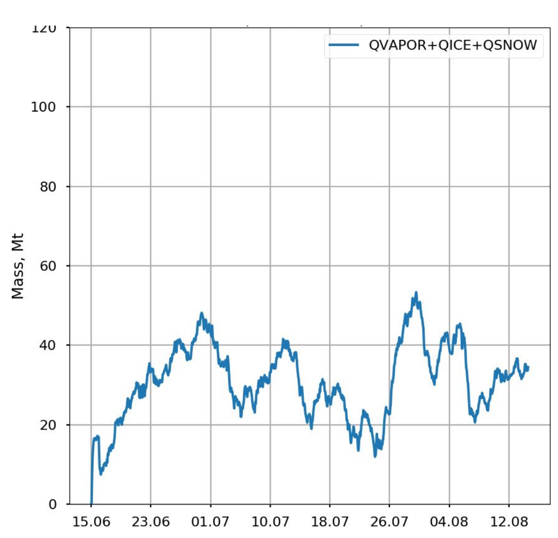

Fig. 6. Difference in total stratospheric water mass (Mt) as a function of time in the runs with volcanic eruption and without.

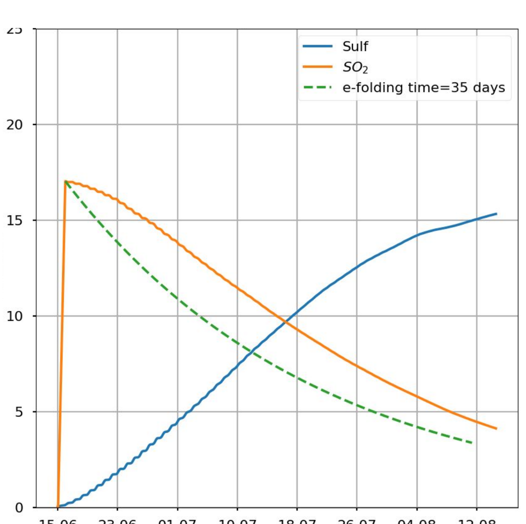

Fig. 7. Mass of SO_2 and Sulfate aerosol (Mt) as a function of time.

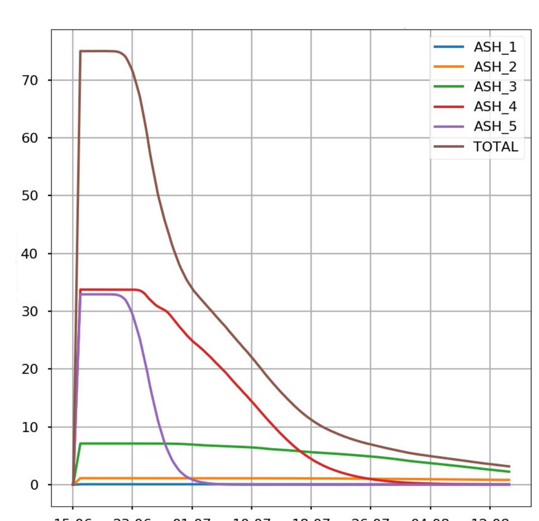

Fig. 8. Mass (Mt) of ash in each 5 bins and total as a functions of time.

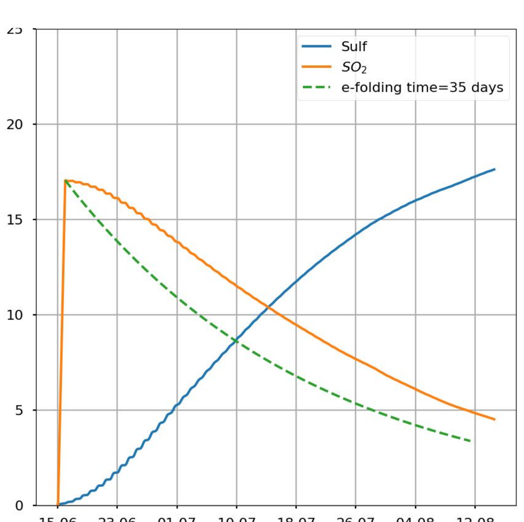

Fig. 9. Mass of SO_2 and Sulfate aerosol (Mt) as a function of time.

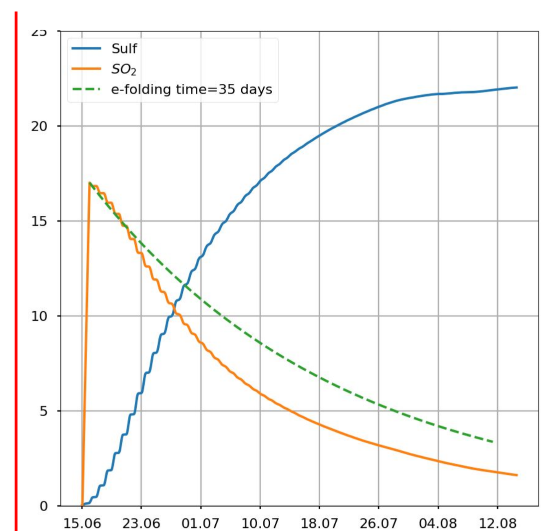

Fig. 10. Mass of SO_2 and Sulfate aerosol (Mt) as a function of time.

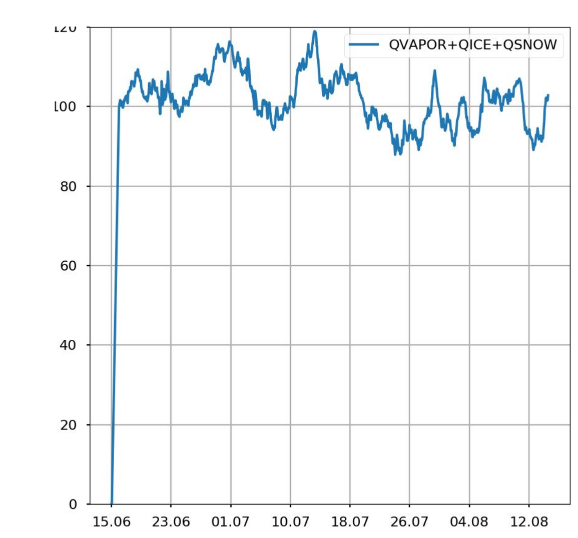

Fig. 11. Difference in total stratospheric water mass (Mt) as a function of time in the runs with volcanic eruption and without.

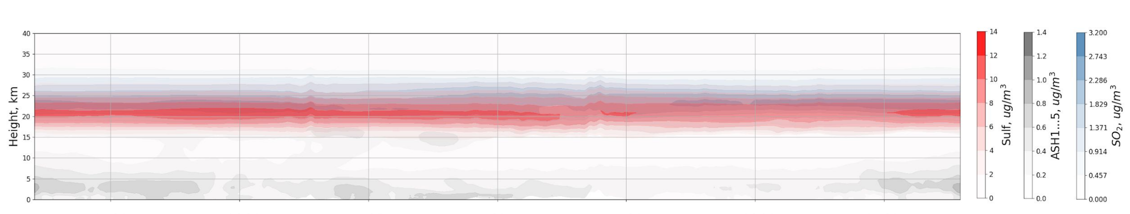

Fig. 12a. Averaged across the equatorial latitude belt slab (0°-15° N) concentrations of Ash, SO_2 and sulfate (ug/m^3) as a function of longitude and height in two month after the eruption.

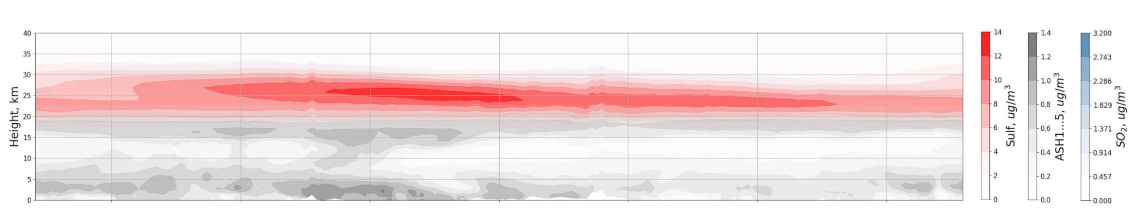

Fig. 12b. Averaged across the equatorial latitude belt slab (0°-15° N) concentrations of Ash, SO_2 and sulfate (ug/m^3) as a function of longitude and height in two month after the eruption.

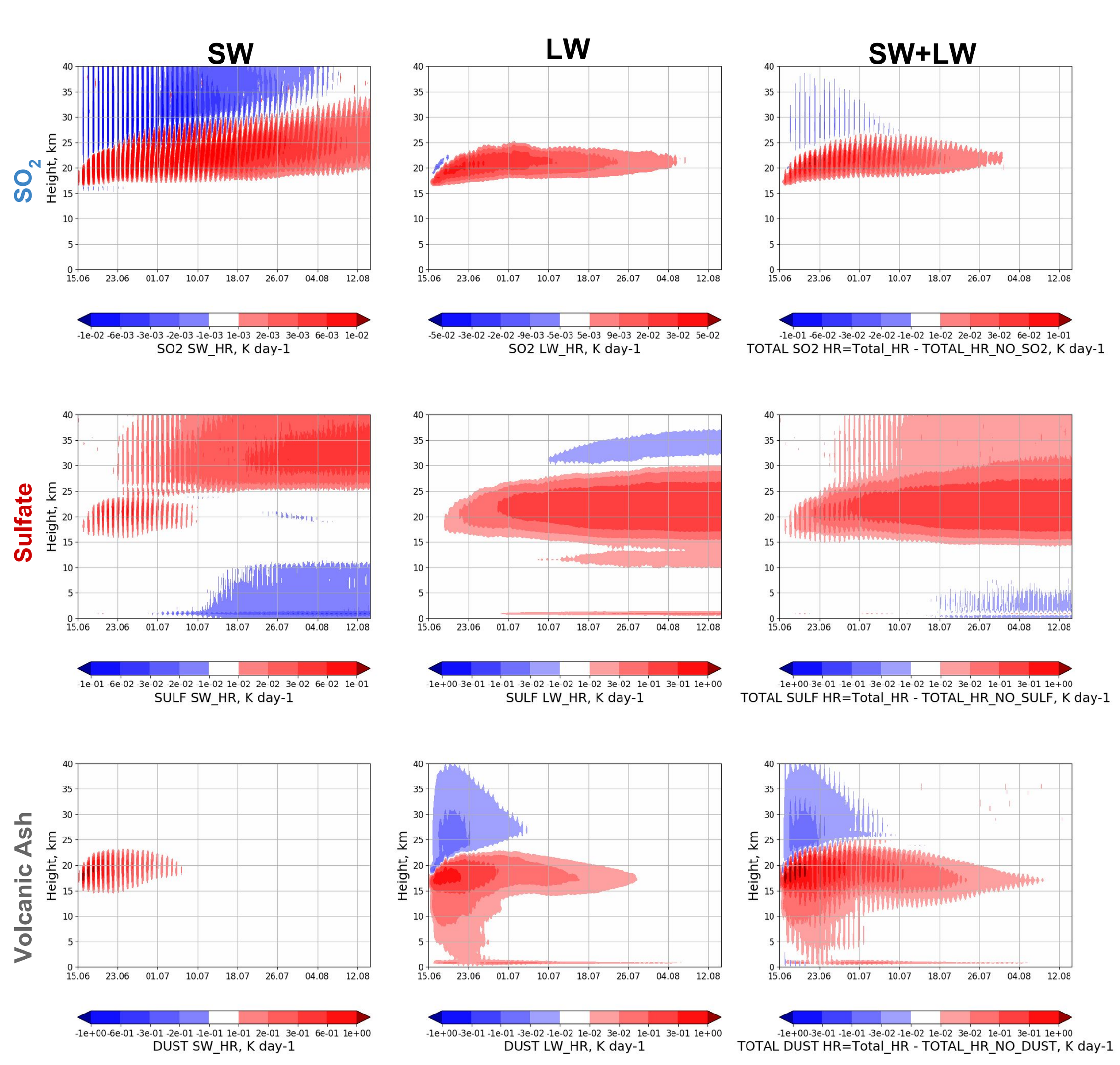

Fig. 13a. Averaged across the equatorial latitude belt slab (0°-15° N) SO_2, Sulfate, Ash heating rates (K/day) as function of time and height.

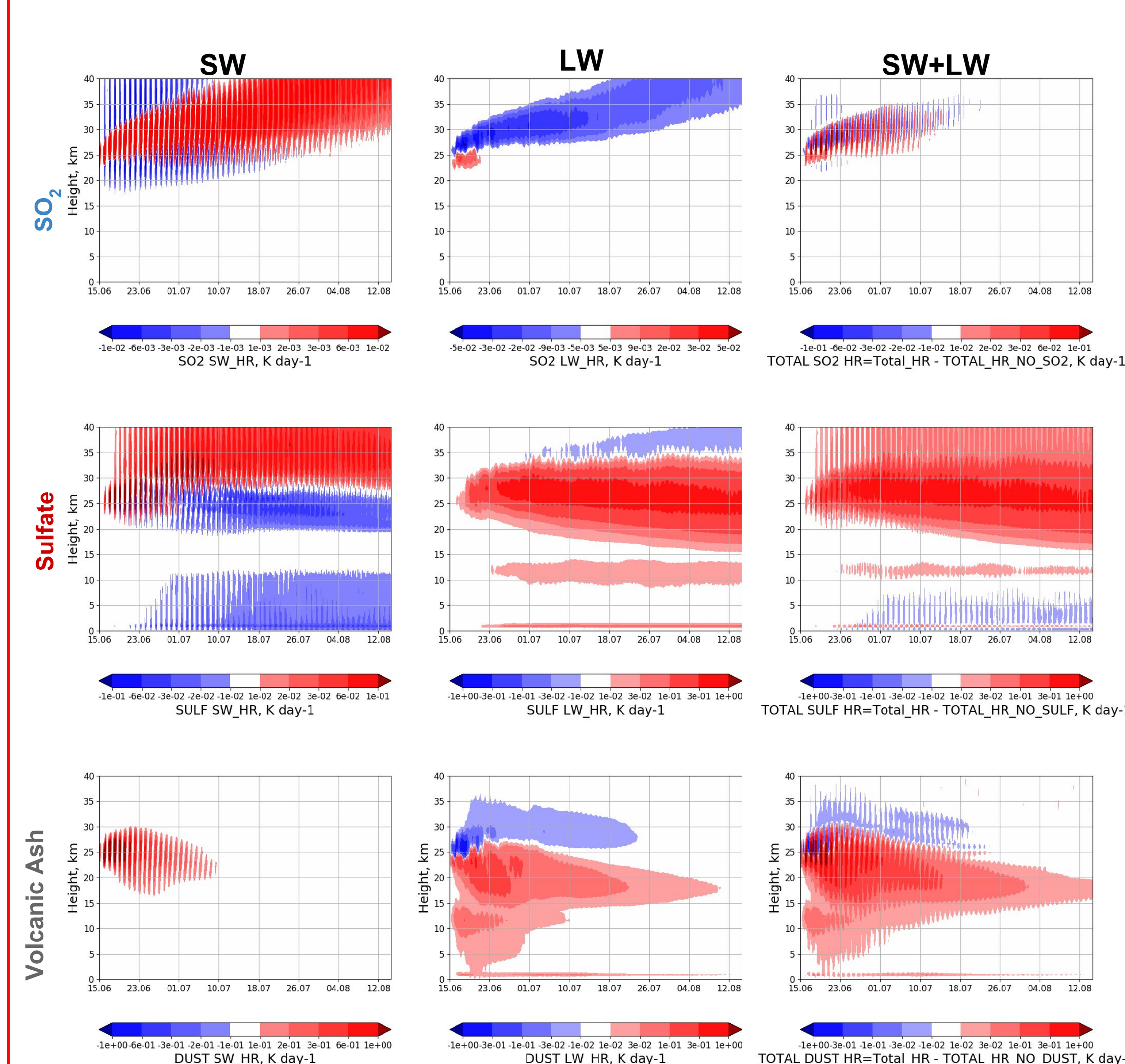

Fig. 13b. Averaged across the equatorial latitude belt slab (0°-15° N) SO_2, Sulfate, Ash heating rates (K/day) as function of time and height.

Conclusions

1. We have simulated the initial stage of volcanic plume after volcanic injections at 17 and 24 km, respectively (**Fig. 1**).
2. We have simultaneously injected water vapor, ash, SO_2 (**Fig. 2 & 3**) and have calculated vertical lifting (**Fig. 4**) and horizontal transport of volcanic plume accounting for the radiative effect in SW and LW of all of the ingredients: SO_2, ash, water vapor, and sulfate. The radiative effects of these components are calculated using double radiative calls with and without corresponding component.
3. The AOD in 17 km emission case is in a better agreement with observations that one in 24 km case (**Fig. 5**).
4. Differential radiative heating and gravitational deposition lead to a separation of ash, SO_2 and sulfate plumes (**Fig. 12a & 12b**) with the SO_2 tending to penetrate into the Mesosphere. The plume evolution, especially effect of water, depends drastically on the initial height of the emission.
5. The sulfate plume rises 5-6 km above the level of initial injection (**Fig. 4**) and its equilibrium height is sensitive to the injection level and strongly affects the horizontal dispersion of a volcanic cloud.
6. The LW heating caused by SO_2 is qualitatively different for the 17 and 24 km emissions because of competing effects of LW spectral absorption by SO_2 plume and ozone layer (**Fig. 13a &13b**).
7. For the eruptions releasing material just above the tropopause practically all water lost to sedimentation as ice and snow (**Fig. 6**). There is no long-term effect of water vapour on the evolution of the plume. The above-tropopause injections warm the tropopause and increase the cross-tropopause water transport in the stratosphere in a month after the eruption.
8. For the eruptions releasing material well above the tropopause most of the water remains in the plume (**Fig. 11**). Water accelerates the SO_2 conversion into sulfate by 20-25% (**Fig. 9** and **10**) affecting vertical distribution of SO_2 and sulfate. The radiatively heated water plume rises to the top of stratosphere and has a tendency to penetrate into the mesosphere.

Acknowledgments

1. The modifications of the radiative code were done by AER's Eli Mlawer, Mike Iacono, and Karen Cady-Pereira.
2. This research was supported by KAUST and used the resources of the KAUST Supercomputing Center.

Contacts

georgiy.stenchikov@kaust.edu.sa,
alexander.ukhov@kaust.edu.sa,
sergey.osipov@kaust.edu.sa